Current Biology 24, 1199–1211, June 2, 2014 ©2014 The Authors http://dx.doi.org/10.1016/j.cub.2014.04.007

Article

Local Control of Intestinal Stem Cell Homeostasis by Enteroendocrine Cells in the Adult *Drosophila* Midgut

Alessandro Scopelliti,[1,3] Julia B. Cordero,[1,3,*] Fengqiu Diao,[2] Karen Strathdee,[1] Benjamin H. White,[2] Owen J. Sansom,[1] and Marcos Vidal[1,*]

[1]The Beatson Institute for Cancer Research, Garscube Estate, Switchback Road, Glasgow G61 1BD, UK

[2]Laboratory of Molecular Biology, NIMH, 35 Convent Drive, MSC 4035, Bethesda, MD 20892-4035, USA

Summary

Background: Enteroendocrine cells populate gastrointestinal tissues and are known to translate local cues into systemic responses through the release of hormones into the bloodstream.

Results: Here we report a novel function of enteroendocrine cells acting as local regulators of intestinal stem cell (ISC) proliferation through modulation of the mesenchymal stem cell niche in the *Drosophila* midgut. This paracrine signaling acts to constrain ISC proliferation within the epithelial compartment. Mechanistically, midgut enteroendocrine cells secrete the neuroendocrine hormone Bursicon, which acts—beyond its known roles in development—as a paracrine factor on the visceral muscle (VM). Bursicon binding to its receptor, DLGR2, the ortholog of mammalian leucine-rich repeat-containing G protein-coupled receptors (LGR4-6), represses the production of the VM-derived EGF-like growth factor Vein through activation of cAMP.

Conclusions: We therefore identify a novel paradigm in the regulation of ISC quiescence involving the conserved ligand/receptor Bursicon/DLGR2 and a previously unrecognized tissue-intrinsic role of enteroendocrine cells.

Introduction

The epithelium of the *Drosophila* adult midgut is replenished by dedicated stem cells [1, 2]. Intestinal stem cells (ISCs) proliferate to self-renew and give rise to an undifferentiated progenitor—the enteroblast—which differentiates into specialized enteroendocrine cells and enterocytes. While enterocytes and enteroblasts have been directly involved in the regulation of midgut homeostasis [3, 4], a local role of enteroendocrine cells within this tissue remains unknown. In mammals, the current evidence implicates enteroendocrine cells as neuroendocrine cells, which provide systemic signals by releasing hormones into the circulation [5].

Mammalian leucine-rich repeat-containing G protein-coupled receptors (LGRs) have emerged as central players in stem cell biology in the recent years. LGR5 is a stem cell marker in the intestine, skin, and stomach, whereas LGR6 labels stem cells in the skin and LGR4 has broader expression domains [6]. However, their biological role remains largely unknown. The current evidence indicates that LGRs act as agonists of canonical Wnt signaling within epithelia to promote proliferation and stem cell maintenance [6]. Paradoxically, growing evidence correlates loss of function mutations in LGR receptors with cancer development [7–10].

Drosophila LGR2 (DLGR2), encoded by the *rickets* (*rk*) gene, represents the single ortholog of mammalian LGR4, LGR5, and LGR6. DLGR2 is activated by its only described ligand, the tanning hormone Bursicon [11, 12]. Described functions of Bursicon and DLGR2 are restricted to developmental processes such the regulation of postmolting cuticle expansion and hardening, as well as wing maturation after eclosion [11, 13].

In this study, we report a local, tissue-autonomous role of the midgut enteroendocrine cells in the control of ISC quiescence during homeostatic conditions. This paracrine mechanism is mediated by the expression of Bursicon in enteroendocrine cells, activating its receptor, DLGR2, which is expressed in the visceral muscle (VM), leading to increased cyclic AMP (cAMP) levels and restrained expression of the epidermal growth factor (EGF)-like growth factor Vein. Our results demonstrate a novel paradigm in the regulation of adult intestinal homeostasis involving a tissue-intrinsic role of enteroendocrine cells, which may apply to multiple stem cell systems.

Results

DLGR2 Is Expressed in the Adult Midgut Visceral Muscle

Consistent with their developmental role, Bursicon and DLGR2 are highly expressed in the pupal and adult molts [13]. However, our recently developed rk^{pan}-*gal4* reporter [14] revealed *rk* expression within the VM of pupal and adult midguts (Figures 1A and 1B and Figure S1B available online). DLGR2 expression within the VM was confirmed with a reporter for the VM-derived EGF-like ligand *vein* [15] (Figure 1B) and a GFP trap for *viking/Collagen IV* (Figure S1F). Additionally, a rk^{pan}-*gal4*-driven lineage tracing system [16] (see the Experimental Procedures) labeled VM cells only, even after 30 days of adult life tracing (Figure S1A). Quantitative RT-PCR (qRT-PCR) from whole mature adult midguts confirmed detectable *dlgr2/rk* transcript expression (Figure 1C), suggesting that DLGR2 could have a role in adult midgut homeostasis. Importantly, VM-targeted knockdown of *rk* by RNAi (how^{ts}>*dlgr2-IR* and *mef2*>*dlgr2-IR*) resulted in decreased transcript levels in adult midguts (Figure 1C). Altogether, our evidence suggests that *rk* is expressed by the VM that surrounds the midgut epithelium. Since the VM is an important component of the *Drosophila* ISC niche [17, 18], we next investigated the functional role of DLGR2 in the adult midgut.

Loss of DLGR2 or Its Ligand Bursicon Function Results in Intestinal Hyperproliferation

The posterior *Drosophila* midgut grows during the first 5 days of adult life, after which it enters homeostasis, characterized by slow cell turnover and relative quiescence of the ISCs [19]. We examined posterior midguts from control and

[3]Co-first author

*Correspondence: j.cordero@beatson.gla.ac.uk (J.B.C.), m.vidal@beatson.gla.ac.uk (M.V.)

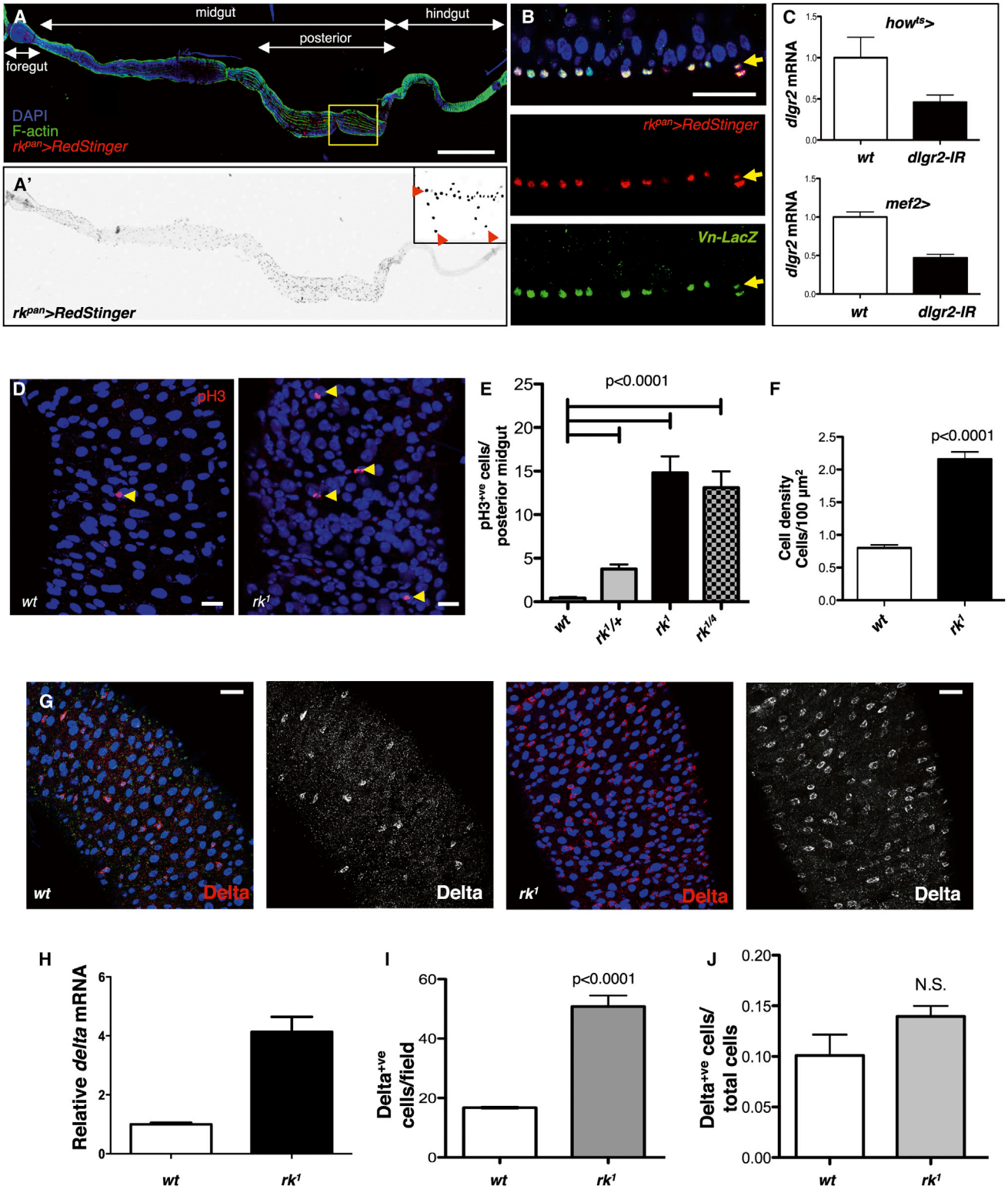

Figure 1. *rk/dlgr2* Is Expressed in the VM and Directs Stem Cell Quiescence

(A) Confocal projection of an adult *rk*^{pan}*>RedStinger* midgut. The different segments of the gut are labeled. The boxed area represents the region imaged for all experiments unless otherwise indicated. Phalloidin (green) labels F-actin. Unless otherwise noted, DAPI (blue) labels all cell nuclei. (A′) shows the RedStinger signal as an inverted grayscale image. The inset shows a representative confocal section displaying both longitudinal and circular RedStinger^{+} VM nuclei (arrowheads). Scale bar, 200 μm.

(B) Confocal longitudinal cross-section from a *rk*^{pan}*>RedStinger; vein-LacZ* midgut. Arrows point to a line of VM nuclei double labeled with *rk*^{pan}*>RedStinger* (red) and *vein-LacZ* (green). Scale bar, 20 μm.

(legend continued on next page)

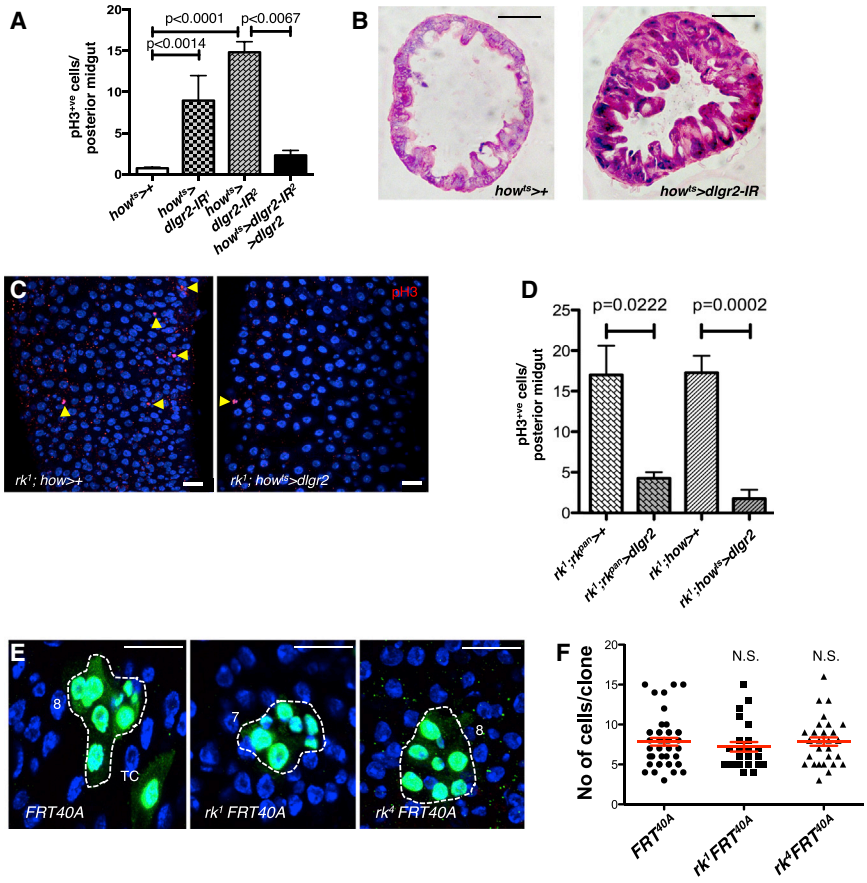

Figure 2. *rk/dlgr2* from the VM Is Required to Drive Stem Cell Quiescence in the Adult *Drosophila* Midgut

(A) Quantification of ISC proliferation in posterior midguts from animals subject to knockdown of *dlgr2* from the VM (*how^{ts}>dlgr2-IR*) and coexpressing *dlgr2-IR* and a *dlgr2* rescue transgene (*how^{ts}>dlgr2-IR; dlgr2*).

(B) Hematoxylin and eosin (H&E) staining of paraffin-embedded sections from 14-day-old posterior midguts as in (A). Note the hypercellularity and epithelial multilayering in *dlgr2* knockdown midguts. Scale bar, 20 μm.

(C) Representative confocal projections of adult midguts from *rk* animals with (right) and without (left) overexpression of *dlgr2* in the VM and stained for pH3 (red; arrows). Scale bar, 20 μm.

(D) Quantification of ISC proliferation in posterior midguts from animals as in (C). *dlgr2* overexpression under the *rk* domain (*rk^{pan}>dlgr2*) or within the VM (*how^{ts}>dlgr2*) rescued the hyperproliferative phenotype of *rk* midguts.

(E) MARCM control or *rk* mitotic clones (GFP labeled; outlined) in posterior midguts with the indicated genotypes. The number of cells in each representative clone is indicated. TC, single-cell transient clone. Scale bar, 20 μm.

(F) Quantification of the number of cells per clone in posterior midguts of the indicated genotypes. Clonal size distribution is presented as a dot plot with the mean clonal size ±SEM indicated in red. N.S., not statistically significant.

See also Figure S1.

loss-of-function *rk* mutants at 10–14 days of adult life. Unlike controls, *rk* mutant midguts displayed ISC hyperproliferation (Figures 1D and 1E), increased cellularity (Figure 1F), and epithelial multilayering (Figure S1C and Movies S2 and S3). We also noted that *rk* midguts displayed increased number of Delta$^+$ ISCs (Figures 1G and 1I), which was confirmed by a marked transcriptional upregulation of *delta* (Figure 1H). The increase in the number of ISCs in *rk* midguts is likely due to an enhanced rate of symmetric ISC division. However, that did not occur at the expense of the differentiated populations since the fraction of Delta$^+$ cells remained unchanged (Figure 1J) and cell differentiation appeared to be unaffected (data not shown). Importantly, our results indicate that DLGR2 is required to restrain ISC proliferation.

To comprehensively assess the functional domain of DLGR2 in the midgut, we next selectively knocked down *dlgr2* from the VM of adult animals. Adult VM knockdown of *rk* using two independent RNAi lines (*how^{ts}>dlgr2-IR^1* and *how^{ts}>dlgr2-IR^2*) phenocopied the ISC hyperproliferation and epithelial multilayering observed in whole *rk* midguts without causing developmental defects (Figures 2A, 2B, and S1G). Furthermore, overexpression of a *UAS-rk^{RA}/dlgr2* transgene in *rk* mutant animals using the *rk^{pan}-gal4* driver (*rk^{pan}>dlgr2*) rescued the developmental [14] and adult midgut phenotypes of *rk* animals (Figures 2D and S1G). As expected, overexpression of the rescue transgene within the adult VM increased *dlgr2* mRNA in the midgut (Figure S1E). Importantly, while this overexpression did not modify developmental defects of *rk* animals, it restored ISC quiescence in *dlgr2-IR* and *rk* midguts (Figures 2A, 2C, 2D, and S1G). Finally, clones of *rk* cells generated within the intestinal epithelium showed no significant differences in cell number when compared with control clones (Figure 2E and 2F). Taken together, these results indicate that ISC hyperproliferation in *rk* midguts is due to loss

(C) qRT-PCR for *rk/dlgr2* mRNA levels relative to *rp49* from control midguts or midguts expressing *rk/dlgr2* RNAi in the adult VM by *how-gal4^{ts}* (top) or *mef2-gal4* (bottom).

(D) Representative confocal projections of wild-type (WT) control and *rk* adult midguts stained for pH3 (red; arrows). Scale bar, 20 μm.

(E) Quantification of ISC proliferation in the posterior midguts as in (D). In this and the subsequent pH3 quantification experiments, data from at least two independent experiments is shown; data are presented as average values ± SEM. p values are indicated in each panel.

(F) Quantification of the total number of DAPI-stained cells per projected unit of area (cellularity) in WT controls and *rk* mutant midguts.

(G) Anti-Delta immunostaining (red and gray) in WT control or *rk* mutant adult midguts. Note the increased number of Delta$^+$ cells per field in the *rk* mutants. Scale bar, 20 μm.

(H) Whole-midgut qRT-PCR for *delta* transcript levels relative to *rp49* from WT and *rk* animals.

(I) Quantification of the total number of Delta$^+$ cells per field.

(J) Percentage of Delta$^+$ cells calculated over the total number of cells per projected confocal field in midguts of the indicated genotypes. Note that, in spite of the higher number of total Delta$^+$ cells per field in *rk* midguts, the increase in total cellularity in the mutants yielded no significant differences in the percentage of Delta$^+$ cells.

See also Figure S1 and Movie S2.

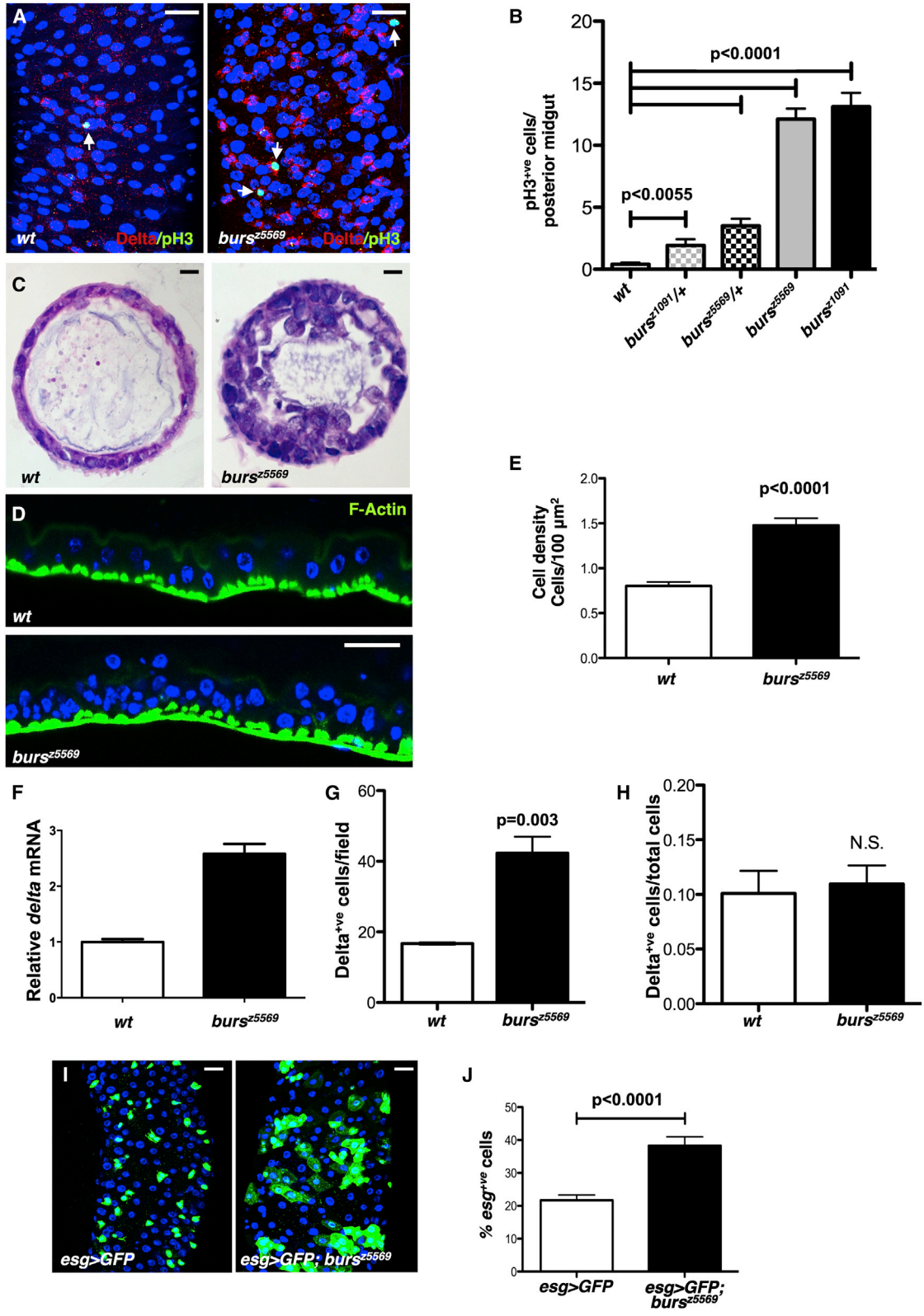

Figure 3. Bursicon Drives Adult Midgut Stem Cell Quiescence

(A) *burs* mutant midguts stained with anti-Delta (red) and anti-pH3 (green; arrows). Scale bar, 20 μm.

(B) Quantification of ISC proliferation in posterior midguts from animals of the indicated genotypes.

(C) H&E staining of paraffin-embedded sections and from posterior midguts of the indicated genotypes. Scale bar, 20 μm.

(D) Confocal transversal sections from posterior midguts of the indicated genotypes. DAPI (blue) and Phalloidin (green) label nuclei and Actin filaments, respectively. Scale bar, 20 μm.

(legend continued on next page)

of gene function within the adult VM and it is independent from developmental defects associated to *rk* loss.

We next addressed the functional role of the DLGR2 ligand, Bursicon [12], in the adult midgut. In the posterior midgut, *burs* loss-of-function mutations fully phenocopied the effects of *rk* mutants (Figures 3A–3H and Movie S4). Furthermore, *burs* midguts displayed significant expansion of the stem and/or progenitor cell population, as visualized by the ISC and/or enteroblast reporter *esg>GFP* [2] (Figures 3I and 3J).

Bursicon/DLGR2 Activates cAMP Signaling in the Visceral Muscle

During development, Bursicon binding to DLGR2 results in increases in cAMP [13]. To test whether Bursicon can regulate DLGR2 activity in the VM, we performed ex vivo cAMP live imaging in posterior midguts using the previously described yellow fluorescent protein (YFP)/cyan fluorescent protein (CFP) fluorescence resonance energy transfer (FRET) sensor *UAS-Epac1-camps* [20], which we expressed within the VM (*how>Epac1*). Treatment with native Bursicon purified from *Carcinus maenas* [21] or hemolymph extracted from freshly eclosed wild-type adults, which contain high titers of Bursicon [22], increased cAMP in the VM in a DLGR2-dependent manner (Figures 4A–4D, S2 and Movie S1). Moreover, hemolymph from freshly eclosed *burs* mutants did not increase cAMP readouts (Figures 4C and S2D). As expected, addition of the adenylyl cyclase activator Forskolin [20] significantly increased cAMP levels independently of DLGR2 (Figures 4C, 4D, S2B, and S2F). Altogether, these results indicate that DLGR2 acts as a receptor for Bursicon in the visceral muscle, leading to the production of cAMP.

To examine for functional effects of suppressing cAMP signaling, we overexpressed the *dunce* cAMP phosphodiesterase [14] or a dominant-negative form of cAMP-dependent protein kinase A (PKA^{inh}) [23] in the VM of adult midguts. Indeed, both transgenes—expected to disrupt the second messenger pathway downstream of DLGR2—reproduced the effects of *rk* loss-of-function mutations or *dlgr2* VM knockdown, leading to ISC hyperproliferation (Figures 4E and 4F).

Bursicon from the CNS Is Not Involved in Intestinal Homeostasis

Bursicon's known expression domain corresponds to a small subset of neurons within the CNS of newly eclosed animals [22] (Figures 5A and S3A). Importantly, we confirmed *burs* expression in whole midguts [5, 24], which in mature adults (10–14 days old) showed transcript levels comparable to those observed in the CNS from late-stage pupae (Figure 5B). CNS-derived Bursicon is responsible for hormone-dependent post-molting events [22]. However, $Burs^+$ neurons apoptose soon after adult maturation [22], and Burs expression in the CNS is undetectable during the stages at which the midgut phenotype becomes evident (Figures S3B and S3C). Consistently, specific knockdown of *burs* using a CNS-restricted *bursicon-gal4* driver [22] reduced *burs* expression in the CNS but not in the midgut (Figures 5A and 5B). This brain-restricted Burs reduction recapitulated *rk* and *burs* developmental defects, but it did not affect midgut homeostasis (Figures 5C–5F), suggesting that the adult midgut phenotype is not dependent on Burs expression in the CNS.

Enteroendocrine Cell-Derived Burs Regulate ISC Proliferation in the Adult Midgut

We next assessed Burs protein expression in the adult midgut by immunofluorescence using a previously described antibody [12, 23] (Figures 6A–6C and S3D). $Burs^+$ population within the posterior midgut belonged to a subset of diploid cells distinct from the esg^+ progenitor population (Figure 6A). Costaining with anti-Prospero antibody, which specifically labels all enteroendocrine cells in the midgut, confirmed that $Burs^+$ cells represented approximately 50% of the enteroendocrine cells in the posterior midgut (n > 150 $Prospero^+$ cells; Figures 6B and 6C).

To directly address the local impact of Burs secretion from enteroendocrine cells, we searched for a *gal4* driver that would reliably label enteroendocrine cells. *voilà-gal4*, which has a *gal4* encoding P element transposon inserted within the *prospero* locus [25], labeled all $Prospero^+$ enteroendocrine cells in the adult midgut (Irene Miguel-Aliaga, personal communication; Figure 6D). *voilà-gal4*-expressing cells in the CNS from newly eclosed animals do not overlap with Bursicon-expressing neurons (Figure S3A). Nevertheless, we used temperature-regulated $voilà\text{-}gal4^{ts}$ to knock down Burs after adult eclosion and maturation and therefore exclude any possible effect on *burs* CNS expression from eclosing animals. The knockdown of Burs within enteroendocrine cells from adult midguts ($voila^{ts}$>*burs-IR*) resulted in midgut-specific downregulation of *burs* transcript (Figure 6E) with nondetectable developmental phenotype in adult animals (Figure 6F). Adult $voila^{ts}$>*burs-IR* midguts displayed ISC hyperproliferation and cell multilayering phenotypes, which phenocopied *burs* mutants (Figures 6G–6I). Altogether, these data indicate that ISC hyperproliferation in *burs* midguts is independent from Bursicon's role in the CNS and is primarily due to intrinsic gene function within adult midgut enteroendocrine cells.

Bursicon Levels in the Midgut Are Regulated during Animal Lifespan

Midguts from young growing or aging animals are characterized by relatively high ISC proliferation [17, 19]. Interestingly, such young or old proliferating midguts showed lower levels of *burs* mRNA when compared to midguts from mature homeostatic animals, which are relatively quiescent (Figure 6J). The fraction of enteroendocrine-expressing Burs did not change significantly during the normal lifespan (50.6% in 3-day-old [n = 150] and 43.7% in 30-day-old [n = 57] animals). These results suggest that, while the number of enteroendocrine cells expressing *burs* is rather constant,

(E) Quantification of the total number of DAPI-stained cells per projected unit of area (cellularity) in WT controls and *burs* mutant midguts.
(F) Whole-midgut qRT-PCR for *delta* transcript levels relative to *rp49* from WT and *burs* animals.
(G) Quantification of the total number of $Delta^+$ cells per field.
(H) Percentage of $Delta^+$ cells calculated over the total number of cells per projected confocal field in midguts of the indicated genotypes. As in *rk* midguts, the increase in total cellularity in *burs* mutants yielded no significant differences in the percentage of $Delta^+$ cells.
(I) *burs* mutant midguts combined with the ISC and/or enteroblast reporter *esg>GFP*. *burs* midguts displayed increased number of $esg>GFP^+$ cells relative to control midguts. Scale bar, 20 μm.
(J) Quantification of the percentage of $esg>GFP^+$ cells in WT controls and *burs* midguts.
See also Movie S4.

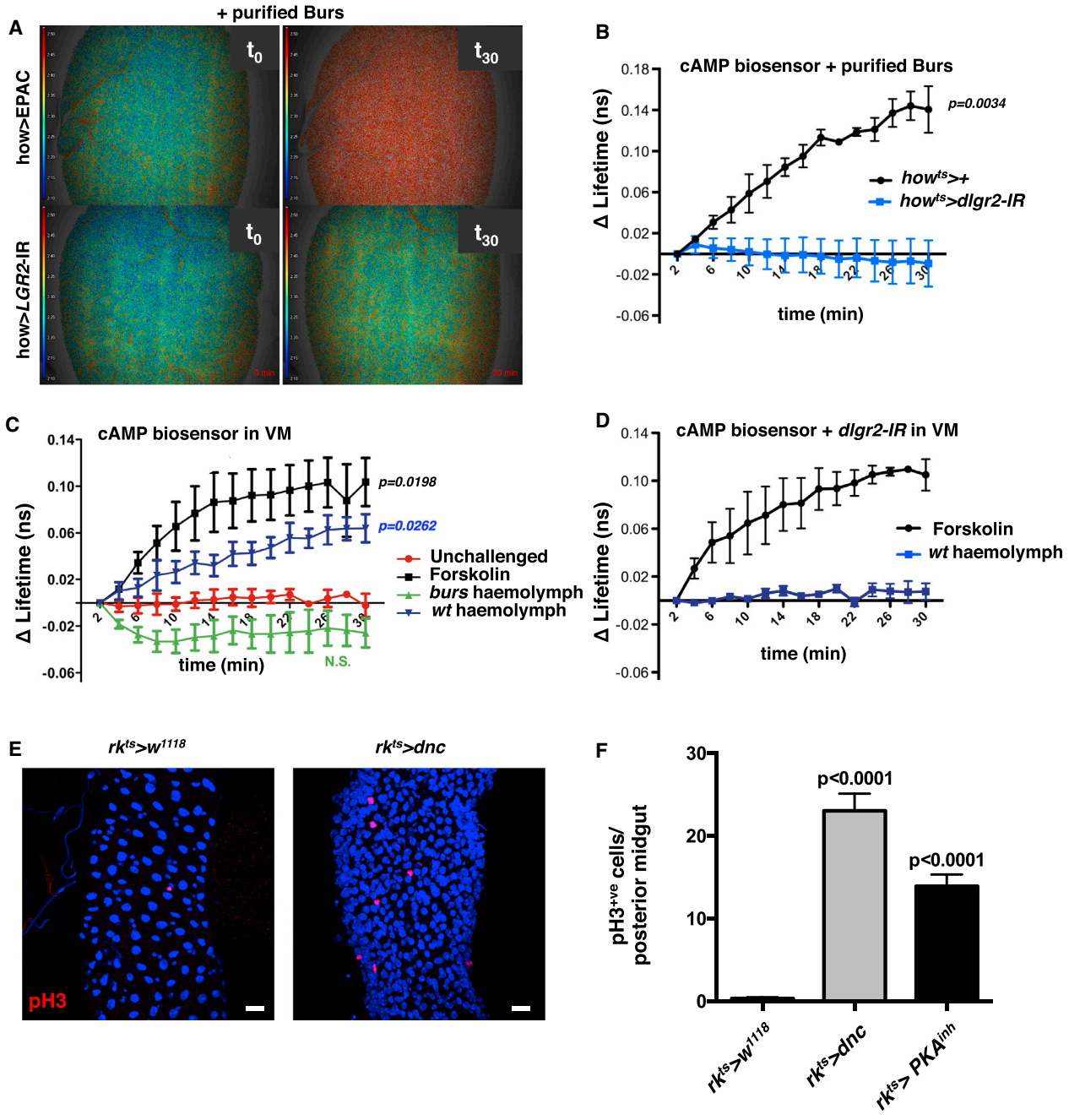

Figure 4. Bursicon Increases VM cAMP via DLGR2

(A–D) Time-lapse FLIM-FRET of Epac1-camps biosensor activation in the VM.

(A) The first (t_0) and last (t_{30}) frames from Movie S1 are shown. The color scale represents levels of cAMP (blue, low; red, high).

(B–D) The different treatments were quantified, and midguts were imaged over the indicated time frame (see the Experimental Procedures). Increases in the fluorescence lifetime indicate increases in cAMP content. Each time point represents the mean from three biological repeats; each quantified in five regions per field shown in Figure S2. Treatment with purified *Carcinus maenas* Bursicon (B), Forskolin (positive control), and WT, but not $burs^{z5569}$ hemolymph (C), increased cAMP concentration within the VM. The effect of purified Bursicon and WT hemolymph was prevented by *dlgr2* knockdown (D). p values from a two-way ANOVA with Bonferroni correction are shown.

(E) Representative confocal projections of adult midguts with the indicated genotypes stained for pH3 (red).

(F) Quantification of ISC proliferation in the posterior midguts from animals of the indicated genotypes. Note the hyperproliferation of midguts expressing the cAMP phosphodiesterase *dunce* or the dominant-negative form of PKA within the *rk* domain.

See also Figure S2.

the levels of *burs* within these cells are regulated. Moreover, *burs* expression in the midgut negatively correlated with its proliferative state during normal lifespan (Figure 6J). To further test Bursicon's functional relevance in regulating ISC proliferation, we overexpressed *burs* in the enteroendocrine cells ($voila^{ts}$>*burs*; Figures S3E and S3G) and examined the effect of this manipulation on ISC proliferation. Midguts coexpressing *burs* and *burs-IR* in enteroendocrine cells

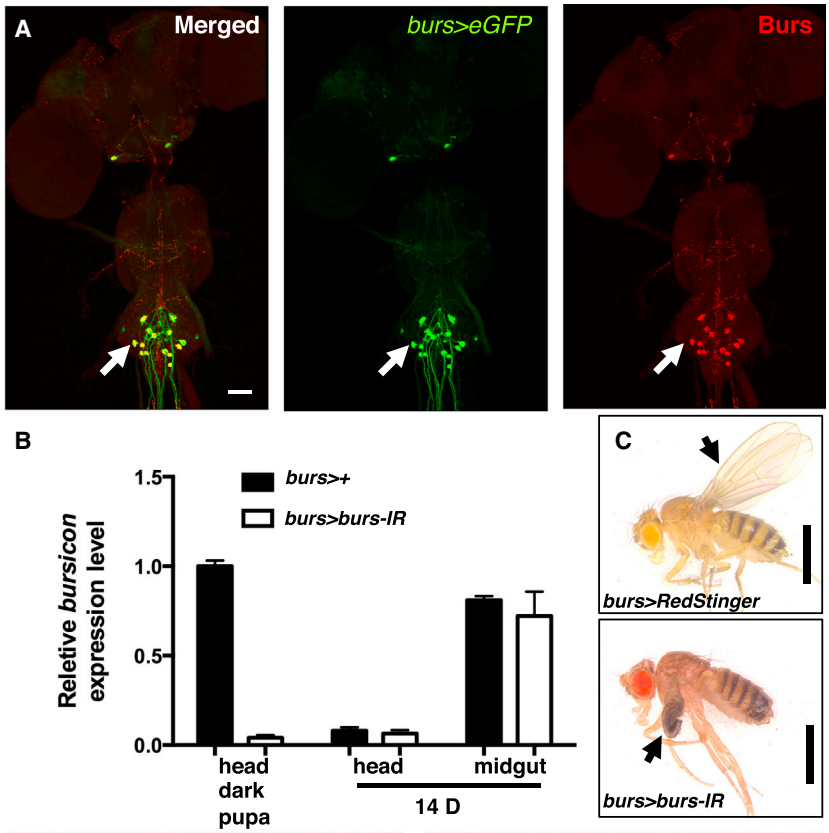

Figure 5. Bursicon from the CNS Does Not Affect Adult Midgut Defects

(A) A *burs-gal4* driver recapitulates Burs expression in the CNS of newly eclosed adult, as shown with double labeling of Burs (red) and *bursG4>eGFP* (green). Scale bar, 50 μm.

(B) qRT-PCR for levels of *burs* transcript relative to *rp49* from heads and midguts from *burs>+* (controls) or *burs>burs-IR* animals. Note that *burs* expression was high in the heads from dark pupae and in the midguts from mature (10- to 14-day-old) adults. *burs* levels were very low in the heads from mature adults. *burs-gal4*-driven RNAi for *burs* effectively knocked down burs in the heads of dark pupae, but not in the midguts from mature adults.

(C) Adult fly micrographs from control (*burs> RedStinger*) and *burs>burs-IR* animals. Note the wing inflation defects (arrow) in the lower panel, characteristic of *burs* mutants. Scale bar, 1mm.

(D and E) Representative confocal images of 10- to 14-day-old midguts from animals with the reported *burs>RedStinger* (D; control) and *burs>burs-IR* (E). Note that the *burs-gal4* line did not drive expression in the posterior midgut (D′) or any other gut segment (data not shown). Arrows label $pH3^+$ cells (green). Scale bar, 50 μm.

(F) Quantification of the number of $pH3^+$ cells in posterior midguts as in (D) and (E).

See also Figure S3.

(*voila*^{ts}*>burs-IR; burs*) displayed suppressed ISC hyperproliferation (Figure 6H). Remarkably, in direct contrast to the *burs* loss-of-function phenotype, overexpression of *burs* suppressed ISC proliferation in both young growing and aging midguts (Figures 6K–6M). We did not observe changes in *burs* transcript levels upon nutrient starvation (data not shown) or enterocyte damage induced via pathogenic infection with *Pseudomonas entomophila* (*Pe*) (Figure S4E). These results suggest that *burs* expression is not regulated upon acute stress. Nevertheless, overexpression of *burs* suppressed ISC proliferation upon damage of the intestinal epithelium by pathogenic infection with *Pe* (Figure S4). Altogether, the age-dependent modulation of *burs* levels and the gain-of-function results further support Bursicon's role driving homeostatic ISC quiescence in the adult *Drosophila* midgut.

Burs/DLGR2/cAMP Signaling Regulates Niche-Derived Growth Factor Vein

We next examined the underlying molecular mechanisms involved in Burs/DLGR2-mediated control of ISC proliferation. We took a candidate-based approach and looked at potential cell-autonomous targets of Burs/DLGR2 in the midgut. Therefore, we analyzed transcript levels of VM-derived factors *wnt/wingless* (*wg*), *unpaired* (*upd*), and *egf/vein* (*vn*) [15, 18, 19, 26, 27]. qRT-PCR from whole *burs*, *rk*, and *how*^{ts}*>dlgr2-IR* adult midguts revealed 3- to 4-fold upregulation of the EGF-like ligand *vn*, which was confirmed with a *vn-LacZ* genetic reporter (Figures 7A–7D).

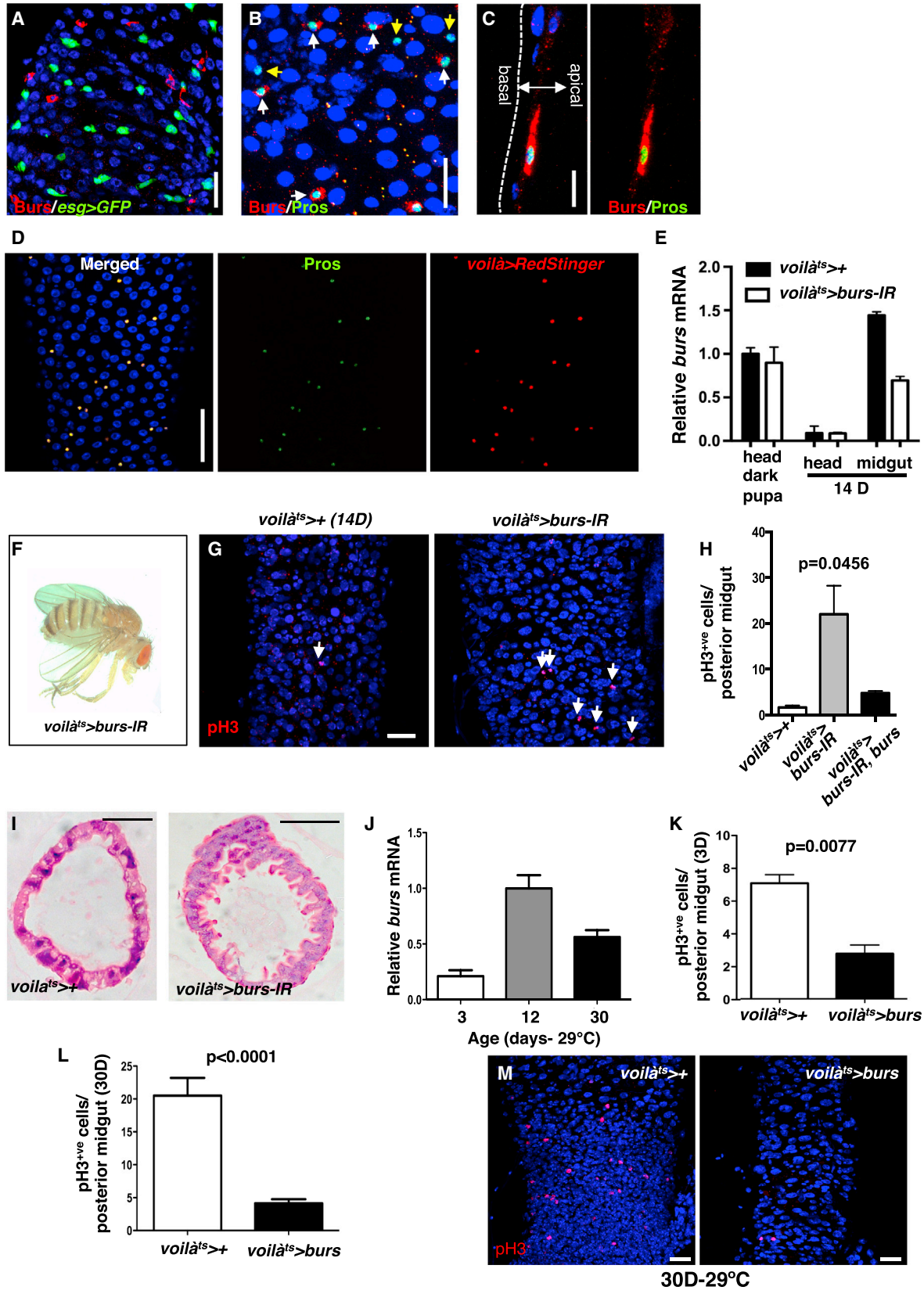

Figure 6. Burs Produced by Enteroendocrine Cells Directs Adult Midgut Stem Cell Quiescence

(A) Confocal projection of a posterior adult midgut stained with anti-Burs (red). *esg>GFP* (green) labels ISCs and/or enteroblasts. Scale bar, 20 μm.
(B) Adult posterior midgut stained with anti-Burs (red) and anti-Prospero (green). White and yellow arrows highlight Prospero^{+}/Burs^{+} and Prospero^{+}/Burs^{-} cells, respectively. Scale bar, 20 μm.

(legend continued on next page)

Previous studies indicated that acute overexpression of Vein in the VM is sufficient to drive ISC hyperproliferation [15, 18, 27]. Moreover, we confirmed that 3- to 4-fold upregulation of *vn* in the VM, which was obtained by a weak expression of *how^{ts}>vn* at 22°C, was sufficient to phenocopy the ISC hyperproliferation of *rk* and *burs* midguts (Figures S5A and S5B).

Our results indicated that Burs/DLGR2 signal via cAMP in the VM. Consistently, the adult VM overexpression of *dunce* or PKA^{inh} displayed increased *vn* expression (Figure 7E).

Vein/EGFR Mediates ISCs Proliferation Downstream of Burs/DLGR2

Given the connection between Burs/DLGR2/cAMP signaling and Vn production in the VM, we next addressed the functional dependency of the ISC hyperproliferation phenotype of *rk* and *burs* mutants on Vn/EGFR signaling. Reduction of *vn* by different genetic loss-of-function mutant combinations, or VM-selective knockdown of *vein* by RNAi suppressed ISC hyperproliferation in *rk*- and *burs*-deficient midguts (Figures 7F, 7G, and S5C). Furthermore, *burs* midguts either heterozygous for a loss-of-function allele of EGFR (*EFGR^{top1}*) or overexpressing a dominant-negative form of EGFR within stem and/or progenitor cells (*esg^{ts}>EGFR^{DN}*) displayed a significantly suppressed ISC hyperproliferation (Figures 7H and S5D). Together, these results indicate that Burs/DLGR2/cAMP signaling directs ISC quiescence in homeostatic midguts, at least in part by downregulating *vn* expression within the VM and therefore suppressing EGFR signaling activation in ISCs (Figure 7I).

Discussion

Bursicon Acts in Adult Midgut Homeostasis

Bursicon, also known as the tanning hormone, has been studied for decades due its essential role as the last hormone in the cascade of Ecdysis [13]. In all invertebrate metazoa, this endocrine cascade is fundamental to coordinate molting events during animal lifetime, and in holometabolous insects, such as *Drosophila*, it control metamorphosis. Fly gene expression data [5, 24] suggest that the endocrine hormones and their cognate receptors involved in key stages of development may have other roles during adult animal life. However, these functional roles are largely unknown. Our study is the first to demonstrate a role of Bursicon beyond development.

We postulate a model (Figure 7I) in which Bursicon from enteroendocrine cells in the posterior midgut acts through DLGR2 to increase the production of cAMP within the VM, a mesenchymal ISC niche. This signaling limits the production of niche-derived, EGF-like Vein, leading to ISC quiescence. We detected Burs protein expression via immunolabeling in approximately 50% of the enteroendocrine cells of the posterior midgut, which appeared in stochastic spatial distribution within the most posterior segment of the adult midgut [28, 29]. Given that the percentage of enteroendocrine cells expressing Burs remained constant, it is likely that Burs expression might label a subtype of enteroendocrine cells within the midgut.

Our evidence indicates that *burs* mRNA levels are upregulated in the midgut during the phase of relative ISC quiescence in mature animals under homeostatic conditions. Conversely, during the phase of growth of the young immature gut or the dysplastic phase of the aging gut—both characterized by relative high rates of ISC proliferation—*burs* levels were relatively low, and *burs* overexpression was sufficient to suppress ISC proliferation. Therefore, our results provide the first demonstration of a tissue-intrinsic role of enteroendocrine cells, which drives homeostatic stem cell quiescence in the adult *Drosophila* midgut. Future studies should further characterize the upstream mechanisms controlling Burs production in the midgut, which might be linked to the yet undefined events involved in the regulation of overall tissue size and proliferation.

Enteroendocrine Cells as Modulators of the Stem Cell Niche

Enteroendocrine cells are well known for their ability to mediate interorgan communication via hormone secretion into the bloodstream [5, 24]. Our results demonstrate a novel, local role for enteroendocrine cells as paracrine regulators of stem cell proliferation. Such a mechanism could be phylogenetically conserved and take place in the mammalian intestine and other tissues of the gastrointestinal tract. This may therefore represent an unappreciated but yet important function of these cells beyond their conventional endocrine role.

LGR Receptors as Inhibitors of Stem Cell Proliferation

Mammalian LGRs are thought to drive ISC proliferation acting as receptors for the Wnt agonists R-spondins [30], which are unrelated to Bursicon and absent in the fly genome. Accordingly, we did not detect changes in either Wg levels or signaling in *burs* or *rk* mutant midguts (Figure S6).

Unexpectedly for a Wnt agonists and positive regulators of ISC proliferation, recent studies suggest that LGRs can act as tumor suppressors in colorectal cancer [7–9]. Moreover,

(C) High-magnification transverse confocal section depicting a Prospero^{+}/Burs^{+} cell. The apical-basal axis of the epithelium (arrow) is oriented from right to left. Scale bar, 20 μm.
(D) *voilà-gal4* labels all enteroendocrine cells in the adult *Drosophila* midgut: *voilà-gal4*-driven RedStinger (red; right) recapitulates the expression pattern of enteroendocrine cells stained with anti-Prospero (green; middle). Colocalization between both markers is shown in yellow (left). Scale bar, 50 μm.
(E) qRT-PCR for levels of *burs* transcript relative to *rp49* from heads or midguts from *voila^{ts}>+* (controls) or *voila^{ts}>burs-IR* animals. Note that *burs* expression was knocked down in midguts, but not in heads.
(F) *voila^{ts}>burs-IR* animals did not display developmental defects.
(G) *voila^{ts}>burs-IR* animals displayed midgut ISC hyperproliferation as shown by anti-pH3 staining (red; arrows).
(H) Quantification of ISC proliferation in midguts from the indicated genotypes.
(I) H&E staining of paraffin-embedded sections from 10-day-old posterior midguts of the indicated genotypes. Note the hypercellularity and epithelial multilayering in *burs* knockdown midguts. Scale bar, 20 μm.
(J) qRT-PCR for *burs* transcript levels relative to *rp49* from whole midguts of WT animals of the indicated ages. Note the age-dependent regulation of *burs*.
(K and L) Quantification of ISC proliferation in posterior midguts from animals of the indicated genotypes and ages. Overexpression of Burs in enteroendocrine cells via *voila^{ts}-gal4* suppressed ISC proliferation of 3-day-old growing (K) and 30-day-old aging (L) midguts.
(M) Posterior midguts from 30-day-old adults as in (L) stained with anti-pH3 (red). Note the reduced number of pH3^{+} cells in *burs* overexpressing midguts. Scale bar, 20 μm.
See also Figures S3 and S4.

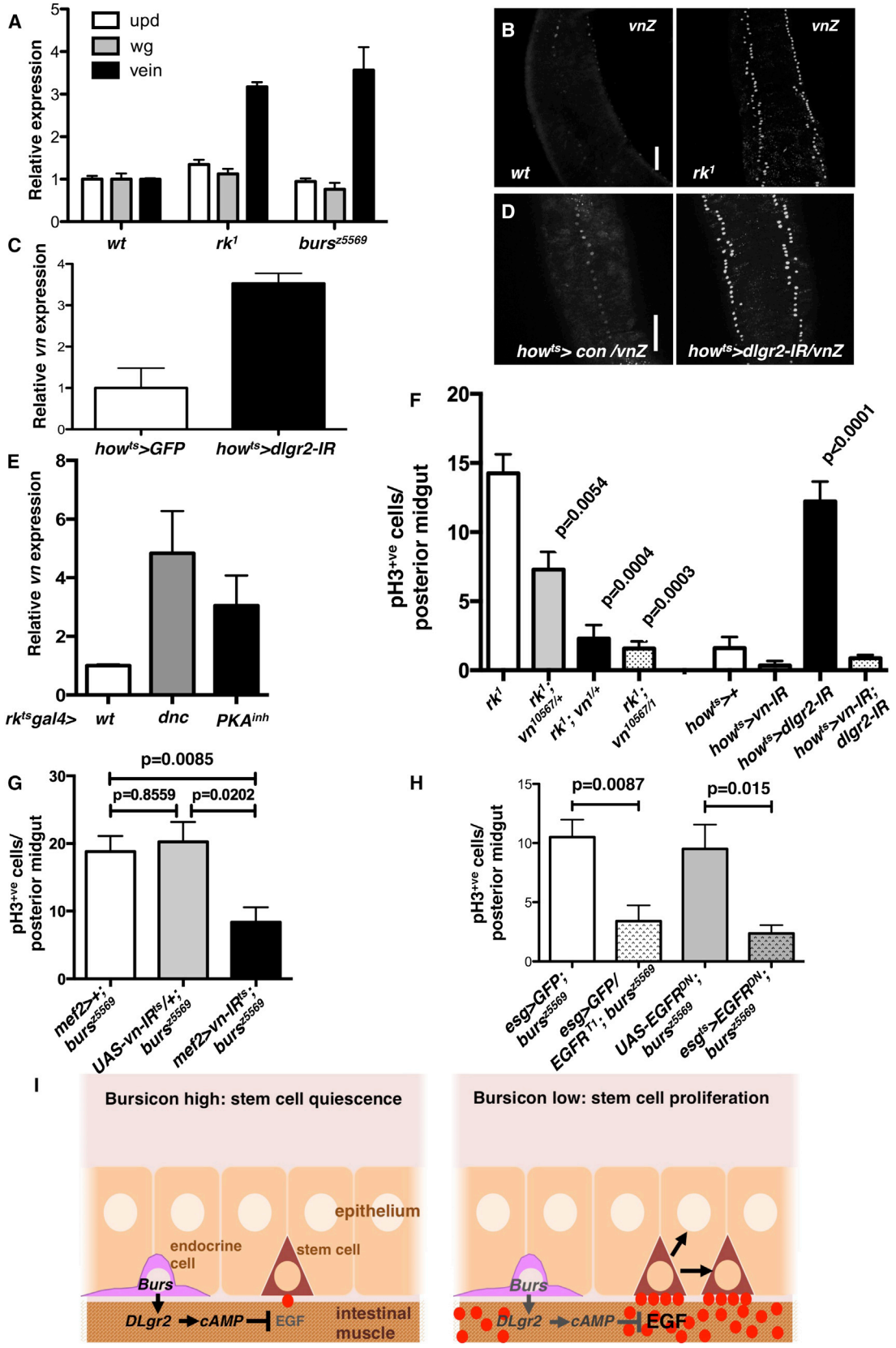

Figure 7. Vn and EGFR Mediate ISC Hyperproliferation in rk and *burs* Midguts

(A) qRT-PCR for *wg*, *upd*, and *vn* transcripts levels relative to *rp49* from WT, rk^1, and $burs^{z5569}$ whole midguts.

(B) *vn* expression in 10- to 14-day-old WT and *rk* mutant midguts visualized with a *vn-LacZ* reporter. Scale bar, 40 μm.

(legend continued on next page)

mammalian LGRs have also been shown to be activated by alternative ligands [31] and promote cAMP signaling after the binding of yet unknown ligand(s) [32, 33]. Therefore, it is likely that an unidentified functional homolog of Bursicon may act as an additional LGR ligand in mammals, driving ISC quiescence by regulating mitogenic signals from the surrounding niche as described here. Remarkably, DLGR2 shows closer sequence homology to the still poorly characterized LGR4 [34] (Figure S5F), which—consistent with our *Drosophila* data—is expressed by the murine intestinal smooth-muscle layers [35] and can signal via cAMP production [32, 33]. Consistent with our model, a recent study correlates loss-of-function mutations in LGR4 with multiple types of human epithelial carcinomas [10]. Therefore, our results uncovered a novel biological role for LGRs, which is likely to impact mammalian stem cell research by providing a mechanistic framework for the so far correlative mammalian evidence toward a potential role of LGRs as tumor suppressor genes.

Altogether, our results demonstrate a novel paradigm in the regulation of intestinal homeostasis involving the conserved ligand/receptor Bursicon/DLGR2 and a previously unrecognized tissue-intrinsic role of enteroendocrine cells, which may provide insights into other stem cell based systems.

Experimental Procedures

Fly Husbandry

Flies were maintained on standard molasses medium in 12 hr light-dark cycles. Adults of the desired genotypes were collected within 24–72 hr of eclosion and then switched to the desired temperature. Food was changed every 2 days. Only female flies were used in this study. Crosses were done at 25°C except when using the TARGET system [36], which involves temporal regulation of Gal4 activity by temperature-sensitive Gal80 ($Gal80^{ts}$).

Experimental Conditions

Unless otherwise indicated, adults of the desired experimental genotypes were aged for 10–14 days at 25°C.

Animals carrying UAS transgenes under the control of the TARGET system [36] were incubated to develop at 18°C and shifted after adult maturation (4–24 hr after eclosion) to 29°C, for 3, 10–14, or 30 days depending on the experiment and as specified in each figure and corresponding figure legend. When not specified, the incubation time was 10–14 days.

Fly Stocks

Further information on *Drosophila* genes and stocks are available from FlyBase (http://flybase.org/). The stock w^{1118} (Bloomington #6326) was used as control strain.

The following fly stocks lines were obtained from the Vienna Drosophila RNAi Center (VDRC) and the Bloomington Stock Center:

w; cn, bw, rk^1 (Bloomington #3589)
w; rk^4 (Bloomington #3590)
UAS-RedStinger (Bloomington #8547)
G-trace (Bloomington #28281)
Vn[10567] (Vn-LacZ) (Bloomington #11749)
Vn[1] (Bloomington #7292)
Actin5C-gal4 (Bloomington #4414)
UAS-burs-IR (VDRC #102204/kk)
UAS-dlgr2-IR^1 (VDRC #904/GD)
UAS-dlgr2-IR^2 (VDRC #105360/kk)
UAS-vein RNAi (VDRC #109437/kk)

The following lines were previously described:

rk^{pan}gal4 [14]
$burs^{z5569}$ [37]
$burs^{z1091}$ [37]
voilà-gal4 [25]
how-gal4 [38]
mef2-gal4 [19]
UAS-dunce [39]
UAS-PKA^{inh} [40]
UAS-$EGFR^{DN}$ (a kind gift from M. Freeman)
$EGFR^{top1}$ (a kind gift from M. Mlodzik)

DLGR2 and Burs Transgene Constructs

cDNA fragments encoding full-length *$dlgr2^{RA}$* and *burs* gene products were cloned into the pUAST vector. Sequenced constructs were injected into $w^{-/-}$ embryos using standard P element transformation technique.

RNA Extraction and qRT-PCR

Total RNA was extracted using standard TRIZOL method or RNAeasy mini kit (QIAGEN) followed by DNase treatment (QIAGEN). cDNA synthesis was performed with the High-Capacity cDNA reverse transcription kit (Applied Biosystems), and MAXIMA SYBR GREEN Master Mix (Fermentas) was used for qPCR according to the manufacturer's instructions. Data were extracted and analyzed using Applied Biosystems 7500 software version 2.0 and Prism GraphPad software. Expression of the target genes was measured relative to that of *RpL32* (rp49). Results represent the average from three technical replicates for each of three independent biological replicates ±SEM. Primers used can be found in Table S1.

Tissue Imaging

Immunofluorescence

Tissues were dissected in PBS and fixed for 30–90 min in 4% paraformaldehyde (Polysciences). Longer fixation times were efficient for Delta staining, while pH3 staining benefited from shorter fixation. After fixation, samples were washed three times in PBS plus 0.1% Triton X-100 (PBST) and incubated in primary antibodies overnight at 4°C. Samples were then washed as described and subjected to secondary antibody staining for 2 hr at room temperature followed by washing and mounting on Vectashield containing DAPI (Vector Laboratories). Primary and secondary antibodies were incubated in PBST plus 0.5% BSA.

Primary Antibodies

The primary antibodies used were as follows: chicken anti-GFP, 1:4,000 (Abcam); mouse anti-Delta, 1:20 (Developmental Studies Hybridoma Bank; DSHB); mouse anti-Prospero, 1:30 (DSHB); rabbit anti-pH3 S10 and S28, 1:100 (Cell Signaling); rabbit anti-Bursicon (α subunit), 1:250; and rabbit anti-β-gal 1:1,000 (Cappel).

Secondary Antibodies

The secondary antibodies used were as follows: goat anti-mouse, goat anti-chicken, or goat anti-rabbit Alexa 488, 1:200 (Invitrogen); and goat anti-mouse or goat anti-rabbit Alexa 594, 1:100 (Invitrogen). F-Actin was visualized with Alexa 488-Phallodin 1:500 (Invitrogen). Nuclei were counterstained with DAPI. Confocal images were collected using a Zeiss 710 Confocal microscope and processed with Zeiss ZEN 2010, ImageJ, or Adobe Photoshop CS.

Histology

Whole midguts were dissected and fixed at 4°C overnight using a 10% formalin solution including 2% Toluidine Blue to improve visualization of the midguts during the embedding and sectioning process. Tissues were

(C) qRT-PCR for *vn* transcripts levels relative to *rp49* in control midguts (*how^{ts}>GFP*) and in midguts expressing *rk/dlgr2* RNAi in the VM (*how^{ts}>dlgr2-IR*).
(D) *vn-LacZ* expression in *how^{ts}>+* and *how^{ts}>dlgr2-IR* midguts.
(E) qRT-PCR for relative *vn* transcripts levels in whole midguts with impaired cAMP signaling through overexpression of *dunce* or dominant-negative PKA in the VM.
(F–H) Quantification of the number of $pH3^+$ cells per posterior midgut from the indicated genotypes. Reduction in Vn suppressed ISC hyperproliferation in *rk*-deficient (F) and *burs*-deficient (G) midguts. Similarly, reduction in EGFR suppressed ISC hyperproliferation in *burs*-deficient midguts (H).
(I) Bursicon secreted from enteroendocrine cells binds its receptor DLGR2 expressed in the visceral muscle, leading to cAMP production, suppression of Vn/EGF, and ISC quiescence.
See also Figures S5 and S6.

then mounted between two layers of 1% agar with the posterior midguts appropriately oriented. Agar-embedded tissues were further incubated in 10% formalin ON and then subjected to paraffin embedding. The paraffin blocks were trimmed in at 10 μm until the beginnings of the orientated midguts were revealed. Serial 4 μm sections of posterior midguts were then cut, placed onto polysine slides, and stained with H&E.

Quantifications and Statistics

ISC proliferation scored by the number of $pH3^+$ cells was restricted to the posterior midgut as indicated by the double arrow in Figure 1A. $pH3^+$ nuclei where counted manually under confocal microscope.

The quantification of the total number of cells (identified by their nuclear DAPI staining), total number of $Delta^+$ cells, and total number of *esg>GFP* cells was restricted to a consistent region of the posterior midgut, which was imaged with a 40× objective and comprised a field of 0.04 mm^2 (boxed area in Figure 1A). The number of $Delta^+$ cells was scored manually, while the total number of cells and esg>GFP cells were quantified with Volocity 3D Image Analysis Software (PerkinElmer).

The data were plotted with Graphpad Prism 5 software. Results represent average values ±SEM. We used a Mann-Whitney test to calculate statistical significance. Eight to 20 posterior midguts from females only were analyzed in each experiment. p values are indicated in each figure panel. p values <0.05 were considered statistically significant.

Clonal Analysis

Recombinant control, rk^1, and rk^4 mutant clones were generated by Flp/FRT-mediated somatic recombination using the MARCM system [41]. Crosses were maintained at 25°C. Adults (3 to 5 days old) of the desired genotypes were selected and subject to three 30 min heat shocks at 37°C in one day. Flies were then incubated at 25°C, and their guts were dissected for analysis 14 days after clonal induction. For scoring of the number of cell per clone, clonal boundaries were determined and the number of nuclei (stained with DAPI) inside each clone was counted. Results were plotted with Graphpad Prism 5 software. The total distribution of clonal sizes is represented as a dot-plot graph with the mean clonal size ±SEM.

Lineage Tracing of $rk^{pan}gal4$

To label rk^{pan}-*gal4* expressing cells and their potential progeny, we used the G-TRACE lineage-tracing system [16] to independently label *rk*-positive cells (rk^{pan}-$gal4^{ts}$/*UAS-RedStinger*) and their potential progeny (rk^{pan}-$gal4^{ts}$/*UAS-Flp/Ubi>stop>eGFP*) over time. If rk^{pan}-*gal4* was labeling ISCs, we would expect to see progressive accumulation of GFP-only cells within the midgut epithelium, corresponding to the progeny of ISCs. However, as mentioned in the main text, we only observed double red and green VM cells labeled, even after 30 days of tracing, and no label within the epithelial compartment (Figure S1A).

Hemolymph Collection

A collecting device made up of a perforated 0.5 ml microtubes inside a 1.5 ml collection tube was used to extract the hemolymph from w^{1118} and bur^{z5569} flies. In brief, 10 to 15 leg- and wing-clipped newly eclosed flies were pooled in the collection device and centrifuged at 12,000 × *g* for 10 min at 4°C. The cleared supernatant was recovered and maintained in dry ice for immediate use or stored at −80°C.

Native Bursicon

A lyophilized sample of HPLC-purified native Bursicon from the shore crab *Carcinus maenas* [21], a kind gift from D. Webster, was suspended in Schneider's Insect media at a concentration of 300 nM. This native Bursicon preparation is bioactive across invertebrate species and induces cuticle tanning in flies [21].

Acquisition of Fluorescent Lifetimes of Epac1-Camps FRET Reporter

Flies of the indicated genotype were dissected in S2 medium to expose the midgut and stretched alongside an ∼10 μl chamber created with double-sided tape on a humidified glass-bottomed 35 mm tissue culture dish (MatTek) and covered with a coverslip. Midguts were imaged on a Nikon Eclipse TE 2000-U microscope using a 60× oil-immersion objective, a suitable filter block for the measurement of CFP lifetime changes based on CFP/YFP FRET (436/20×, T455LP dichroic mirror, 480/40 M), and a 445 nm intensity-modulated LED for illumination. FLIM-FRET was measured by the frequency domain method using the Lambert Instruments fluorescence attachment (LIFA). Fluorescein solution (10 μM) in Tris-Cl (0.1 M; pH >10) was used as reference standard with a known lifetime of 4.0 ns. Data were acquired every minute for 30 min after the addition of 2.5 μl hemolymph, 150 nM purified *Carcinus maenas* Bursicon [21], or 2.5 μl of Forskolin 250 μM as positive control. Each treatment was performed on three biological replicates. Data analysis was performed with FLIM software (version 1.2.12; Lambert Instruments). Reporter activity was quantified in five different visceral muscle regions of interest (ROIs) consistent over the acquisition time for each gut. Data from each ROI were expressed as difference to the basal lifetime and averaged over 2 min. Because these experiments are defined by two parameters (time and genotype treatment), a two-way ANOVA test with Bonferroni correction was applied for assessment of statistically significant differences. p values are indicated in the corresponding figure panels. p values <0.05 were considered statistically significant.

Supplemental Information

Supplemental Information includes six figures, one table, and four movies and can be found with this article online at http://dx.doi.org/10.1016/j.cub.2014.04.007.

Author Contributions

J.B.C., O.J.S., and M.V. formulated the initial hypothesis. J.B.C. initiated the project. A.S., J.B.C., and M.V. designed and performed most of the experiments. K.S. created the UAS-DLGR2 transgene and validated the bursicon RNAi lines. F.D. and B.H.W. provided unpublished reagents and performed the CNS staining. All authors participated in the writing of the manuscript.

Acknowledgments

We thank A.J. Hsueh, J. Ewer, I. Miguel-Aliaga, P. Leopold, B. Edgar, M. Mlodzik, M. Freeman, the VDRC, Bloomington Stock Center, and the Developmental Studies Hybridoma Bank for providing advice, fly lines, and reagents. We especially thank E.M. Dewey and H.W. Honegger for generously sharing the unpublished *UAS-burs* line, D. Whitehead and S. Webster for purified Bursicon, C. Nixon for assistance with histological analysis, and J. Schwarz, M. O'Prey, and D. Strachan for assistance with the FRET and images quantification analysis. We apologize to those whose work could not be cited due to space restrictions. F.D. and B.H.W. are supported by the Intramural Research Program of the National Institute of Mental Health (project 1ZIA-MH-002800). M.V. and O.J.S. are Cancer Research UK investigators (grant number C596/A17196). This work was partly funded by a NC3Rs grant to J.B.C., M.V., and O.J.S. J.B.C. was funded by Marie Curie and EMBO fellowships and is a Dorothy Hodgkin Royal Society Fellow and a Glasgow University Leadership Fellow.

Received: November 22, 2013
Revised: February 27, 2014
Accepted: April 2, 2014
Published: May 8, 2014

References

1. Ohlstein, B., and Spradling, A. (2006). The adult Drosophila posterior midgut is maintained by pluripotent stem cells. Nature *439*, 470–474.
2. Micchelli, C.A., and Perrimon, N. (2006). Evidence that stem cells reside in the adult Drosophila midgut epithelium. Nature *439*, 475–479.
3. Jiang, H., Patel, P.H., Kohlmaier, A., Grenley, M.O., McEwen, D.G., and Edgar, B.A. (2009). Cytokine/Jak/Stat signaling mediates regeneration and homeostasis in the Drosophila midgut. Cell *137*, 1343–1355.
4. Cordero, J.B., Stefanatos, R.K., Scopelliti, A., Vidal, M., and Sansom, O.J. (2012). Inducible progenitor-derived Wingless regulates adult midgut regeneration in Drosophila. EMBO J. *31*, 3901–3917.
5. Lemaitre, B., and Miguel-Aliaga, I. (2013). The digestive tract of Drosophila melanogaster. Annu. Rev. Genet. *47*, 377–404.
6. Barker, N., and Clevers, H. (2010). Leucine-rich repeat-containing G-protein-coupled receptors as markers of adult stem cells. Gastroenterology *138*, 1681–1696.
7. Gong, X., Carmon, K.S., Lin, Q., Thomas, A., Yi, J., and Liu, Q. (2012). LGR6 is a high affinity receptor of R-spondins and potentially functions as a tumor suppressor. PLoS ONE *7*, e37137.
8. de Sousa E Melo, F., Colak, S., Buikhuisen, J., Koster, J., Cameron, K., de Jong, J.H., Tuynman, J.B., Prasetyanti, P.R., Fessler, E., van den Bergh, S.P., et al. (2011). Methylation of cancer-stem-cell-associated

Wnt target genes predicts poor prognosis in colorectal cancer patients. Cell Stem Cell *9*, 476–485.

9. Walker, F., Zhang, H.H., Odorizzi, A., and Burgess, A.W. (2011). LGR5 is a negative regulator of tumourigenicity, antagonizes Wnt signalling and regulates cell adhesion in colorectal cancer cell lines. PLoS ONE *6*, e22733.
10. Styrkarsdottir, U., Thorleifsson, G., Sulem, P., Gudbjartsson, D.F., Sigurdsson, A., Jonasdottir, A., Jonasdottir, A., Oddsson, A., Helgason, A., Magnusson, O.T., et al. (2013). Nonsense mutation in the LGR4 gene is associated with several human diseases and other traits. Nature *497*, 517–520.
11. Baker, J.D., and Truman, J.W. (2002). Mutations in the Drosophila glycoprotein hormone receptor, rickets, eliminate neuropeptide-induced tanning and selectively block a stereotyped behavioral program. J. Exp. Biol. *205*, 2555–2565.
12. Luo, C.W., Dewey, E.M., Sudo, S., Ewer, J., Hsu, S.Y., Honegger, H.W., and Hsueh, A.J. (2005). Bursicon, the insect cuticle-hardening hormone, is a heterodimeric cystine knot protein that activates G protein-coupled receptor LGR2. Proc. Natl. Acad. Sci. USA *102*, 2820–2825.
13. Honegger, H.W., Dewey, E.M., and Ewer, J. (2008). Bursicon, the tanning hormone of insects: recent advances following the discovery of its molecular identity. J. Comp. Physiol. A Neuroethol. Sens. Neural Behav. Physiol. *194*, 989–1005.
14. Diao, F., and White, B.H. (2012). A novel approach for directing transgene expression in Drosophila: T2A-Gal4 in-frame fusion. Genetics *190*, 1139–1144.
15. Jiang, H., Grenley, M.O., Bravo, M.J., Blumhagen, R.Z., and Edgar, B.A. (2011). EGFR/Ras/MAPK signaling mediates adult midgut epithelial homeostasis and regeneration in Drosophila. Cell Stem Cell *8*, 84–95.
16. Evans, C.J., Olson, J.M., Ngo, K.T., Kim, E., Lee, N.E., Kuoy, E., Patananan, A.N., Sitz, D., Tran, P., Do, M.T., et al. (2009). G-TRACE: rapid Gal4-based cell lineage analysis in Drosophila. Nat. Methods *6*, 603–605.
17. Biteau, B., Hochmuth, C.E., and Jasper, H. (2008). JNK activity in somatic stem cells causes loss of tissue homeostasis in the aging Drosophila gut. Cell Stem Cell *3*, 442–455.
18. Biteau, B., and Jasper, H. (2011). EGF signaling regulates the proliferation of intestinal stem cells in Drosophila. Development *138*, 1045–1055.
19. O'Brien, L.E., Soliman, S.S., Li, X., and Bilder, D. (2011). Altered modes of stem cell division drive adaptive intestinal growth. Cell *147*, 603–614.
20. Ponsioen, B., Zhao, J., Riedl, J., Zwartkruis, F., van der Krogt, G., Zaccolo, M., Moolenaar, W.H., Bos, J.L., and Jalink, K. (2004). Detecting cAMP-induced Epac activation by fluorescence resonance energy transfer: Epac as a novel cAMP indicator. EMBO Rep. *5*, 1176–1180.
21. Webster, S.G., Wilcockson, D.C., Mrinalini, and Sharp, J.H. (2013). Bursicon and neuropeptide cascades during the ecdysis program of the shore crab, Carcinus maenas. Gen. Comp. Endocrinol. *182*, 54–64.
22. Peabody, N.C., Diao, F., Luan, H., Wang, H., Dewey, E.M., Honegger, H.W., and White, B.H. (2008). Bursicon functions within the Drosophila CNS to modulate wing expansion behavior, hormone secretion, and cell death. J. Neurosci. *28*, 14379–14391.
23. Luan, H., Lemon, W.C., Peabody, N.C., Pohl, J.B., Zelensky, P.K., Wang, D., Nitabach, M.N., Holmes, T.C., and White, B.H. (2006). Functional dissection of a neuronal network required for cuticle tanning and wing expansion in Drosophila. J. Neurosci. *26*, 573–584.
24. Chintapalli, V.R., Wang, J., and Dow, J.A. (2007). Using FlyAtlas to identify better Drosophila melanogaster models of human disease. Nat. Genet. *39*, 715–720.
25. Balakireva, M., Gendre, N., Stocker, R.F., and Ferveur, J.F. (2000). The genetic variant Voila causes gustatory defects during Drosophila development. J. Neurosci. *20*, 3425–3433.
26. Veenstra, J.A., Agricola, H.J., and Sellami, A. (2008). Regulatory peptides in fruit fly midgut. Cell Tissue Res. *334*, 499–516.
27. Buchon, N., Broderick, N.A., Kuraishi, T., and Lemaitre, B. (2010). Drosophila EGFR pathway coordinates stem cell proliferation and gut remodeling following infection. BMC Biol. *8*, 152.
28. Buchon, N., Osman, D., David, F.P., Fang, H.Y., Boquete, J.P., Deplancke, B., and Lemaitre, B. (2013). Morphological and molecular characterization of adult midgut compartmentalization in Drosophila. Cell Rep. *3*, 1725–1738.
29. Marianes, A., and Spradling, A.C. (2013). Physiological and stem cell compartmentalization within the Drosophila midgut. Elife *2*, e00886.
30. de Lau, W., Barker, N., Low, T.Y., Koo, B.K., Li, V.S., Teunissen, H., Kujala, P., Haegebarth, A., Peters, P.J., van de Wetering, M., et al. (2011). Lgr5 homologues associate with Wnt receptors and mediate R-spondin signalling. Nature *476*, 293–297.
31. Deng, C., Reddy, P., Cheng, Y., Luo, C.W., Hsiao, C.L., and Hsueh, A.J. (2013). Multi-functional norrin is a ligand for the LGR4 receptor. J. Cell Sci. *126*, 2060–2068.
32. Gao, Y., Kitagawa, K., Shimada, M., Uchida, C., Hattori, T., Oda, T., and Kitagawa, M. (2006). Generation of a constitutively active mutant of human GPR48/LGR4, a G-protein-coupled receptor. Hokkaido Igaku Zasshi *81*, 101–105, 107, 109.
33. Luo, J., Zhou, W., Zhou, X., Li, D., Weng, J., Yi, Z., Cho, S.G., Li, C., Yi, T., Wu, X., et al. (2009). Regulation of bone formation and remodeling by G-protein-coupled receptor 48. Development *136*, 2747–2756.
34. Eriksen, K.K., Hauser, F., Schiøtt, M., Pedersen, K.M., Søndergaard, L., and Grimmelikhuijzen, C.J. (2000). Molecular cloning, genomic organization, developmental regulation, and a knock-out mutant of a novel leu-rich repeats-containing G protein-coupled receptor (DLGR-2) from Drosophila melanogaster. Genome Res. *10*, 924–938.
35. Mustata, R.C., Van Loy, T., Lefort, A., Libert, F., Strollo, S., Vassart, G., and Garcia, M.I. (2011). Lgr4 is required for Paneth cell differentiation and maintenance of intestinal stem cells ex vivo. EMBO Rep. *12*, 558–564.
36. McGuire, S.E., Mao, Z., and Davis, R.L. (2004). Spatiotemporal gene expression targeting with the TARGET and gene-switch systems in Drosophila. Sci. STKE *2004*, pl6.
37. Dewey, E.M., McNabb, S.L., Ewer, J., Kuo, G.R., Takanishi, C.L., Truman, J.W., and Honegger, H.W. (2004). Identification of the gene encoding bursicon, an insect neuropeptide responsible for cuticle sclerotization and wing spreading. Curr. Biol. *14*, 1208–1213.
38. Jiang, H., and Edgar, B.A. (2009). EGFR signaling regulates the proliferation of Drosophila adult midgut progenitors. Development *136*, 483–493.
39. Cheung, U.S., Shayan, A.J., Boulianne, G.L., and Atwood, H.L. (1999). Drosophila larval neuromuscular junction's responses to reduction of cAMP in the nervous system. J. Neurobiol. *40*, 1–13.
40. Li, W., Ohlmeyer, J.T., Lane, M.E., and Kalderon, D. (1995). Function of protein kinase A in hedgehog signal transduction and Drosophila imaginal disc development. Cell *80*, 553–562.
41. Lee, T., and Luo, L. (2001). Mosaic analysis with a repressible cell marker (MARCM) for Drosophila neural development. Trends Neurosci. *24*, 251–254.